A&A 661, A77 (2022)
https://doi.org/10.1051/0004-6361/202142839

Astronomy & Astrophysics

An approximate recipe of chromospheric radiative losses for solar flares

J. Hong[1,2], M. Carlsson[3,4], and M. D. Ding[1,2]

[1] School of Astronomy and Space Science, Nanjing University, Nanjing 210023, PR China
e-mail: jiehong@nju.edu.cn
[2] Key Laboratory for Modern Astronomy and Astrophysics (Nanjing University), Ministry of Education, Nanjing 210023, PR China
[3] Rosseland Centre for Solar Physics, University of Oslo, PO Box 1029, Blindern 0315, Oslo, Norway
[4] Institute of Theoretical Astrophysics, University of Oslo, PO Box 1029, Blindern 0315, Oslo, Norway

Received 6 December 2021 / Accepted 11 March 2022

ABSTRACT

Context. Radiative losses in the chromosphere are very important for the energy balance of the Sun. There have been efforts to make simple lookup tables for chromospheric radiative losses in the quiet Sun. During solar flares, the atmospheric conditions are quite different, and the currently available recipe is constructed from semi-empirical models. How these recipes work in flare conditions remains to be evaluated.
Aims. We aim to construct an approximate recipe of chromospheric radiative losses for solar flares.
Methods. We tabulate the optically thin radiative loss, escape probability, and ionization fraction using a grid of flare models from radiative hydrodynamic simulations as our dataset.
Results. We provide new lookup tables to calculate chromospheric radiative losses for flares. Compared with previous recipes, our recipe provides a better approximation of the detailed radiative losses for flares.

Key words. radiative transfer – Sun: chromosphere – Sun: flares

1. Introduction

In the solar atmosphere, radiation plays an important role in the energy balance. The contribution of radiation to the change in the internal energy, often referred to as radiative losses, is quantified as the divergence of the radiative flux:

$$Q_{\rm rad} = -\nabla \cdot \mathcal{F}. \tag{1}$$

A positive value of $Q_{\rm rad}$ means that there is local heating from the extinction of photons, and a negative value indicates local cooling through the emission of photons. In the transition region and corona, the atmosphere is optically thin and the radiative losses can be simplified in the form of

$$Q_{\rm rad} = -\Lambda(T, n_{\rm e}) n_{\rm e} n_{\rm H}, \tag{2}$$

where $n_{\rm e}$ is the electron density, $n_{\rm H}$ is the hydrogen density, and Λ can be calculated under the coronal approximation with the CHIANTI database (Dere et al. 1997; Del Zanna et al. 2021).

However, in the chromosphere, the strong lines are normally optically thick, which means that there is a probability for the energy (in the form of photons) to escape. Carlsson & Leenaarts (2012, hereafter CL12) wrote the radiative loss function from element X at ionization stage m as:

$$Q_{{\rm rad},X_m} = -L_{X_m} E_{X_m} \frac{n_{X_m}}{n_{\rm X}} \frac{n_{\rm X}}{n_{\rm H}} \frac{n_{\rm H}}{\rho} n_{\rm e} \rho, \tag{3}$$

where L_{X_m} is the thin radiative loss function, E_{X_m} is the escape probability, and $\frac{n_{X_m}}{n_{\rm X}}$ is the ionization fraction of element X at ionization stage m. These three parameters are determined empirically from radiative (magneto)hydrodynamic simulations of the quiet Sun. $\frac{n_{\rm X}}{n_{\rm H}}$ is the abundance of element X relative to hydrogen, $\frac{n_{\rm H}}{\rho}$ is the number of hydrogen particles per mass unit, a constant dependent on abundances, and ρ is the mass density. This approximate recipe can reproduce radiative cooling of the quiet Sun very well, and has been included in many radiative (magneto)hydrodynamic codes (e.g., Gudiksen et al. 2011; Bradshaw & Cargill 2013; Wang & Yokoyama 2020).

During solar flares, the chromosphere undergoes drastic changes, with a rapid rise in temperature, electron density, and pressure. The bombardment of the nonthermal electrons can also increase the excitation and ionization rate of neutral hydrogen in the ground level (Fang et al. 1993). With such different local conditions, it is noted that the chromospheric radiative losses in flares are much larger than those in the quiet Sun (Machado et al. 1980; Avrett et al. 1986). The work of Gan & Fang (1990, hereafter GF90) provides a revision to the recipe of Nagai (1980) based on fitting the radiative loss curves of semi-empirical models. The recipe of GF90 has a similar form:

$$Q_{\rm rad} = -f(T)\alpha(z) n_{\rm H} n_{\rm e}, \tag{4}$$

where $f(T)$ is the thin radiative loss function, and $\alpha(z)$ is the probability that the energy escapes from height z.

The recipe of GF90 is constructed over only two semi-empirical models, and it is not clear whether or not these models can cover the variation range of solar flares. In addition, the recipe takes the height variable z as an input, while in actual simulations, the height and thickness of the chromosphere are not necessarily the same as in semi-empirical models. On the other hand, the recipe of CL12 is based on the quiet-Sun atmosphere; how it works during flares remains to be evaluated, and this could

Table 1. Line fluxes and total radiative fluxes of the chromosphere from lines and Lyman continuum in different flare models.

Flare	$\mathcal{F}_{\rm avg}$ (10^7 erg cm^{-2} s^{-1})					$\mathcal{F}^{\rm tot}$ (10^9 erg cm^{-2})				$\Delta\mathcal{F}^{\rm tot}$ (%)			Flare
model	Lyα	Hα	Ca II K	Ca II 8542 Å	Mg II k	detailed	GF90	CL12	this work	GF90	CL12	this work	class [(1)]
Models for fitting													
f10E05d3	5.51	3.42	0.87	0.45	2.55	5.84	7.60	57.29	4.84	30.30	881.55	−17.01	C2.7
f10E10d3	7.07	2.92	0.61	0.35	2.28	5.48	13.67	78.15	5.88	149.37	1325.90	7.34	…
f10E15d3	6.39	2.85	0.65	0.38	1.71	5.48	9.34	86.55	6.80	70.53	1480.13	24.06	…
f10E20d3	4.66	2.99	0.68	0.40	1.79	5.79	7.98	100.48	6.71	37.95	1636.76	15.93	…
f10E25d3	3.44	3.08	0.71	0.42	1.86	5.19	7.50	89.74	5.13	44.72	1630.54	−1.06	…
f10E05d4	3.69	3.22	0.88	0.44	2.28	4.87	6.59	37.22	3.96	35.25	663.58	−18.67	C7.6
f10E10d4	6.96	3.02	0.73	0.39	2.56	6.15	12.22	76.78	6.56	98.93	1149.53	6.68	A8.9
f10E15d4	7.67	2.49	0.54	0.34	1.71	5.19	9.70	81.54	7.64	86.92	1471.62	47.35	…
f10E20d4	6.46	2.69	0.57	0.35	1.77	6.36	8.21	108.33	9.10	28.99	1602.69	43.00	…
f10E25d4	4.71	2.83	0.58	0.36	1.78	6.26	7.36	106.08	6.38	17.66	1595.74	1.91	…
f10E05d5	3.23	2.90	0.81	0.41	2.02	4.12	6.08	26.29	3.24	47.38	537.83	−21.48	C9.2
f10E10d5	6.45	3.05	0.77	0.40	2.56	6.14	11.55	71.84	6.46	88.16	1070.65	5.26	B4.5
f10E15d5	8.10	2.25	0.49	0.32	1.74	4.70	9.77	73.06	7.49	107.63	1453.28	59.19	…
f10E20d5	6.90	2.49	0.52	0.33	1.69	6.23	8.33	83.67	9.20	33.70	1242.40	47.67	…
f10E25d5	5.49	2.64	0.52	0.33	1.70	6.70	7.16	102.43	4.20	6.92	1428.60	−37.30	…
f10E05d6	2.83	2.66	0.76	0.39	1.83	3.61	5.72	20.54	2.74	58.61	469.43	−23.89	C9.8
f10E10d6	6.08	3.05	0.77	0.40	2.56	5.96	11.15	66.55	6.22	87.02	1016.10	4.35	C1.4
f10E15d6	8.47	2.08	0.44	0.29	1.73	4.38	10.60	62.16	7.24	141.69	1317.65	65.14	…
f10E20d6	7.45	2.36	0.50	0.32	1.72	6.07	8.40	71.96	7.76	38.40	1086.18	27.93	…
f10E25d6	6.06	2.53	0.50	0.31	1.62	6.87	7.05	96.32	2.94	2.62	1302.35	−57.26	…
f10E05d7	2.56	2.52	0.73	0.38	1.70	3.29	5.52	17.28	2.41	67.87	425.43	−26.70	C9.9
f10E10d7	5.74	3.04	0.77	0.39	2.51	5.73	10.89	62.02	5.97	90.26	983.12	4.33	C2.1
f10E15d7	8.51	2.04	0.39	0.28	1.74	4.07	24.17	49.62	6.99	494.22	1119.93	71.87	…
f10E20d7	7.97	2.28	0.48	0.31	1.70	5.85	8.23	63.71	5.05	40.67	989.04	−13.69	…
f10E25d7	6.54	2.47	0.49	0.31	1.52	6.89	6.99	89.27	2.35	1.48	1195.81	−65.92	…
Models for test													
f11E15d3	18.18	11.30	1.79	0.76	5.82	26.65	88.13	613.66	58.06	230.69	2202.68	117.88	M7.2
f11E20d4	18.00	13.35	2.13	0.91	4.84	25.43	99.28	633.49	53.25	290.35	2390.70	109.35	M3.2
f11E25d5	15.64	14.11	2.56	1.01	5.49	28.02	58.06	688.50	48.53	107.21	2357.03	73.19	C1.6

Notes. [(1)]Flare class below A1.0 is not labeled.

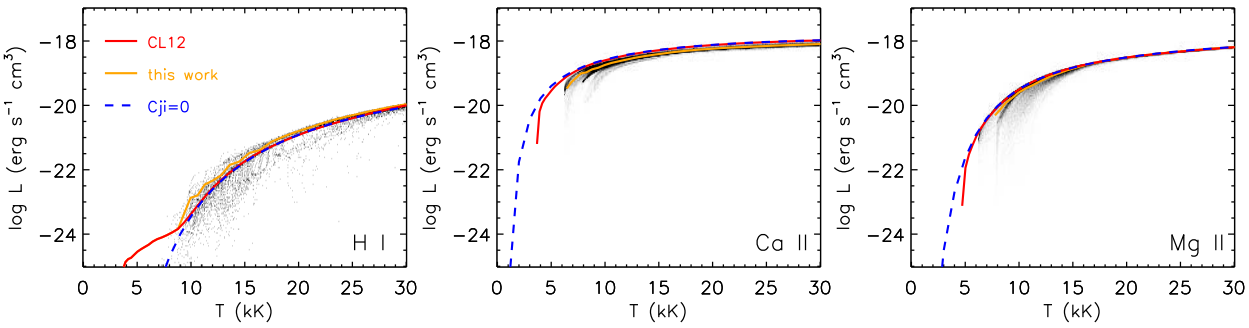

Fig. 1. Probability density function of the thin radiative loss function (H I, Ca II, and Mg II) as a function of temperature. Colored lines show relations from the recipe of CL12 (red), the adopted fit of the PDF (yellow), and cases with negligible collisional deexcitation rates (blue, Eq. (4) of CL12).

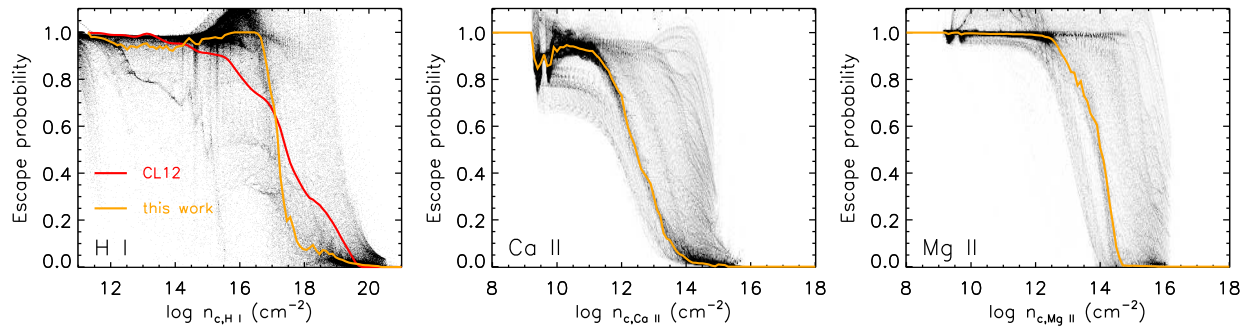

Fig. 2. Probability density function of the escape probability (H I, Ca II, and Mg II) as a function of the column density of the specific ion. Colored lines show relations from the recipe of CL12 (red) and the adopted fit of the PDF (yellow). We note that in the *middle* and *right panels*, the results are plotted as a function of column density of Ca II and Mg II, respectively, and thus we do not plot the results from the recipe of CL12.

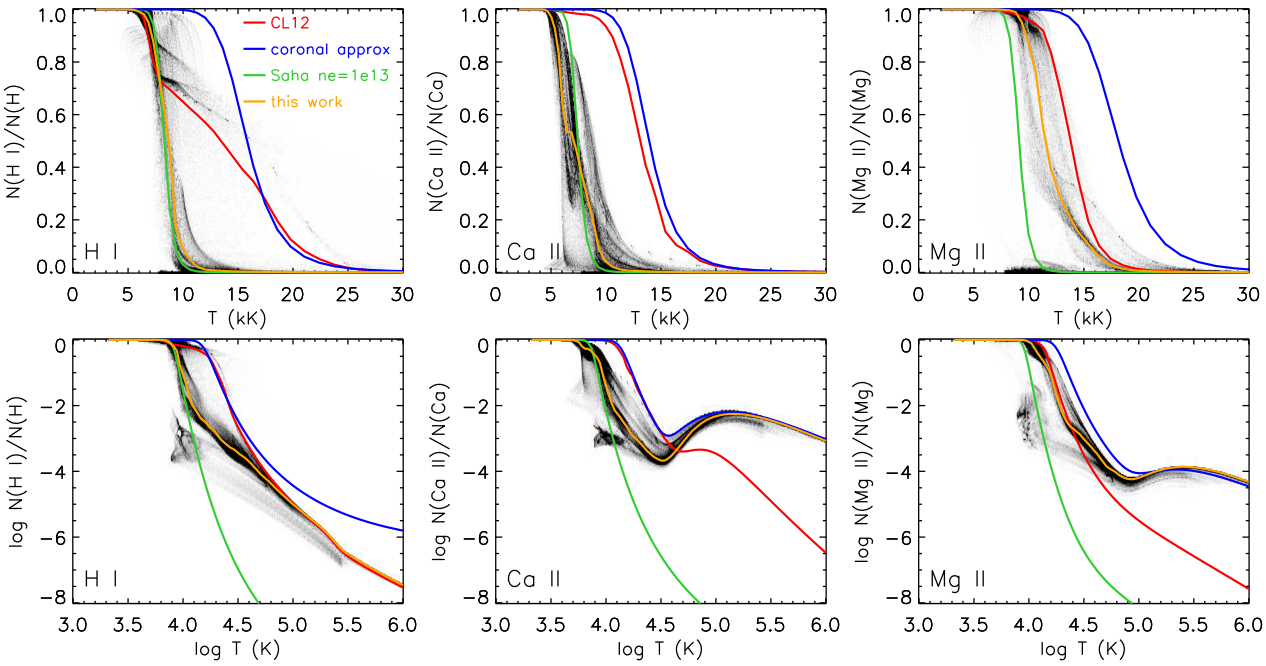

Fig. 3. Probability density function of the population fractions (H I, Ca II, and Mg II) as a function of temperature. The panels in the *upper row* are a zoomed-in view of part of the panels in the *lower row* for the temperature range of $T < 30$ kK. Colored lines show the results from the recipe of CL12 (red), the coronal approximation with a two-level atom (blue), the Saha equation with a constant $n_e = 10^{13}$ cm^{-3} (green), and the adopted fit of the PDF (yellow).

be important given that the atmospheric conditions are quite different. In this paper, we follow the steps in CL12 and redo the fits of the three parameters from a grid of flare simulations. We briefly introduce our method in Sect. 2. The fitting results and comparisons with other recipes are shown in Sect. 3. We give our conclusions in Sect. 4.

2. Method

We employ a grid of 25 flare models generated with the radiative hydrodynamics code RADYN (Carlsson & Stein 1992, 1995, 1997, 2002). The flare loop is assumed to be symmetric; thus half of the loop is modeled as a quarter circle with a 10 Mm length. In each flare model, the initial quiet-Sun atmosphere is heated by a beam of nonthermal electrons injected from the loop top (Allred et al. 2015). The initial temperature at the loop top is 1 MK. The beam of electrons is assumed to have a power-law distribution of energy, as described with three parameters: the electron flux F, the spectral index δ, and the cutoff energy E_c. The electron flux F is a triangular function of time, with 10 s increase and 10 s decrease, and the peak flux is 10^{10} erg cm^{-2} s^{-1} for all models. The spectral index δ varies from 3 to 7, and the cutoff energy E_c varies from 5 to 25 keV. These 25 models are used to fit the three parameters in Eq. (3), and we use another three models with a larger peak electron flux (10^{11} erg cm^{-2} s^{-1}) to test the recipe (see Sect. 3.2). These models are labeled as fn_1En_2dn_3 in Table 1, where the numbers n_1, n_2, and n_3 correspond to the values of log F at peak time, the cutoff energy E_c, and the spectral index δ, respectively. Each simulation is run for 20 s, and the snapshot at every 0.1 s is saved to the output. The RADYN outputs are then fed into RH (Uitenbroek 2001; Pereira & Uitenbroek 2015) to calculate the Ca II and Mg II lines, taking into account the effect of partial frequency redistribution. In RH we assume statistical equilibrium.

The H model atom used in our RADYN simulations is the same as in CL12, but for the Lyman series a Gaussian profile is used instead of a Voigt profile to mimic the effect of partial frequency redistribution (Leenaarts et al. 2012). The Ca II model atom is the same as in CL12 and the Mg II model atom is the same as in Leenaarts et al. (2013).

The radiative losses from H are calculated from the RADYN outputs, and the losses from Ca and Mg are calculated from the RH outputs. We consider contributions from all the H lines between the lowest five energy levels, the Lyman continuum, the Ca II H/K and triplet lines, as well as the Mg II H/K lines. Balmer and higher continua of H are not considered here because they do not comply with the recipe, but we discuss in Sect. 3.4 that their contribution is not negligible and should be modeled properly.

The time-averaged radiation fluxes of various spectral lines from these flare models are summarized in Table 1. In these models, the energy in the chromosphere is mostly dissipated through Lyα, Hα, and Mg II photons (Machado et al. 1980). The flare class is estimated from the synthetic GOES 1−8 Å flux that is calculated following Kerr et al. (2020), with the cross section of the flare loop assumed to be 4×10^{15} cm^2 (a diameter of 1″). We note that in our flare models we only consider heating from nonthermal electrons, and the thermal electrons with an energy below the cutoff energy E_c are all neglected. The coronal emission would be lower than expected without these thermal electrons, which can heat the corona efficiently (Polito et al. 2018). Therefore, the calculated soft X-ray flux, which mainly originates from coronal emissions, would be significantly underestimated if E_c is large enough. Special care must be taken when comparing the flare class of the models with real observations.

3. Results

3.1. Empirical fitting results of the parameters

As shown in Eq. (3), there are three parameters that need to be fitted empirically: the optically thin loss function L_{X_m}, the escape

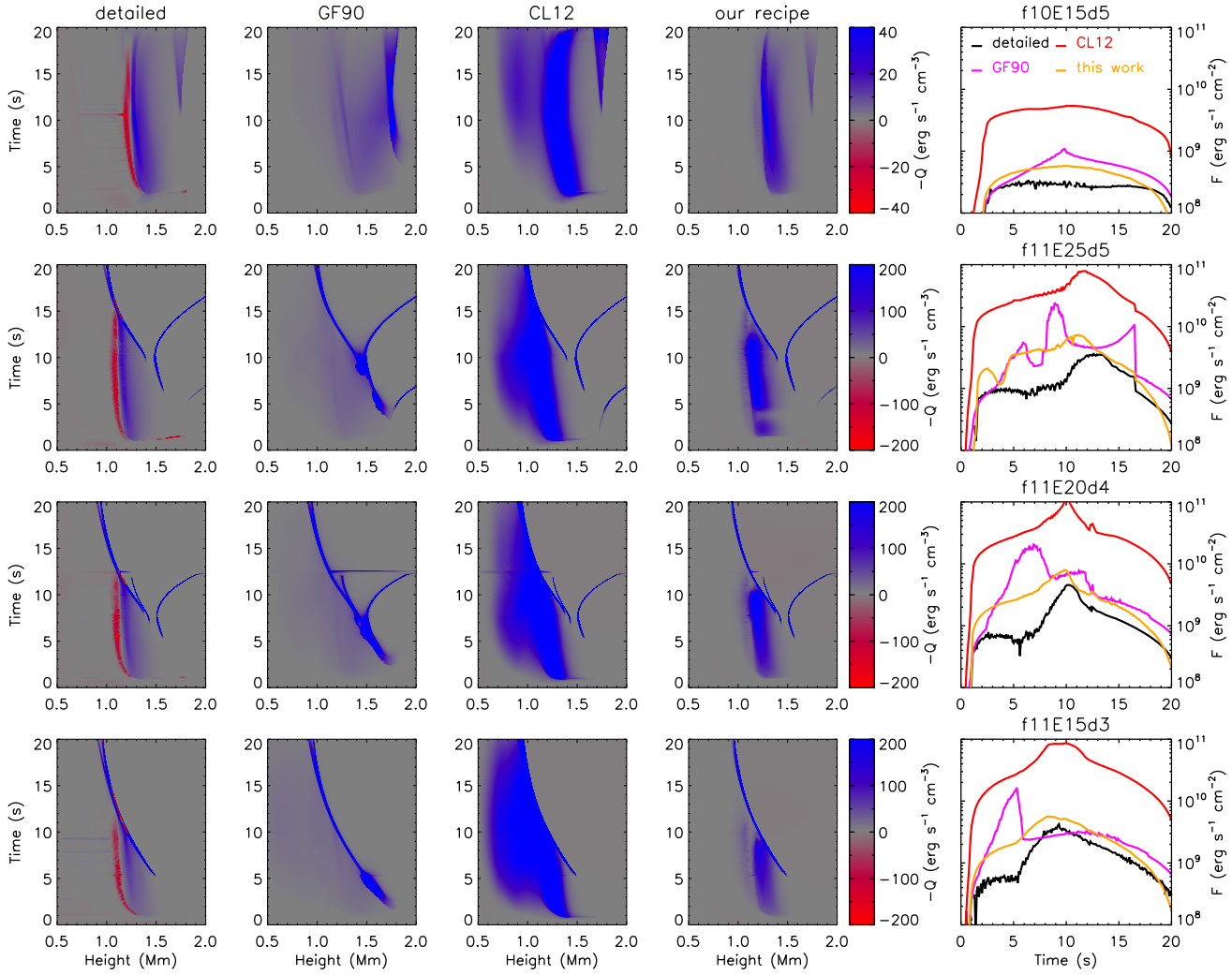

Fig. 4. Comparison of chromospheric radiative losses calculated from detailed solutions and with different approximate recipes for four simulation cases. Blue colors denote radiative cooling, and red colors denote radiative heating. The line plots give comparisons of the evolutions of the radiative cooling rates integrated from 0.5 Mm to 2.0 Mm.

probability E_{X_m}, and the ionization fraction $\frac{n_{X_m}}{n_X}$. The probability density functions (PDFs) of the optically thin loss function are shown in Fig. 1. The radiative losses should be equal to the total collisional excitation from the ground state if the collisional deexcitation rates are small enough, which is the case in the quiet Sun for temperatures above 10 kK (Carlsson & Leenaarts 2012). In flare cases, the fitted curves have similar shapes compared with the results from CL12, despite a larger spread at low temperatures. In addition, the curves for cases with negligible collisional deexcitation rates (calculated from Eq. (4) of CL12) and fitted curves overlap above a temperature much higher than 10 kK.

The PDFs of the escape probability are shown in Fig. 2. In CL12, the escape probability of H I is tabulated as a function of the approximated optical depth of the Lyα line center ($\tau = 4 \times 10^{-14}\, n_{\mathrm{c,H\,I}}$, with $n_{\mathrm{c,H\,I}}$ the column density of H I), while the escape probability of Ca II and Mg II is tabulated as a function of column mass m_{c}. In flare conditions, the Ca II and Mg II atoms in the chromosphere are more likely to get ionized, and thus it is not appropriate to use the column mass to approximate the optical depths of these lines. Therefore, in our recipe we use the column densities of H I, Ca II, and Mg II to tabulate their escape probability. There is a larger spread in the PDFs, and the curve of H I escape probability is steeper than that of CL12. The fitted curves show small dips at low column densities, which is a result of chromospheric condensation regions where the local density is large enough to block photons to some extent.

The PDFs of the ionization fraction are shown in Fig. 3. It is clear that the empirical relations of CL12 no longer hold for typical chromospheric temperatures ($T = 10^4$–10^5 K). In the flaring chromosphere, the increased electron density (in the order of 10^{13} cm^{-3}) has greatly enhanced the collisional rates, and the local atmosphere is driven towards local thermodynamical equilibrium. The fitted curves of H I and Ca II at low temperatures are very close to the Saha equilibrium. At high temperatures ($T > 10^5$ K), the fitted curve of H I follows that of CL12, while the fitted curves of Ca II and Mg II follow that of the coronal approximation with a two-level atom. The humps in the curves of Ca II and Mg II near $T = 10^{5.2}$ K result from dielectronic recombinations.

3.2. Comparison with other recipes

We choose four flare models to test the performance of different recipes. Among the four flare models, the first one (f10E15d5)

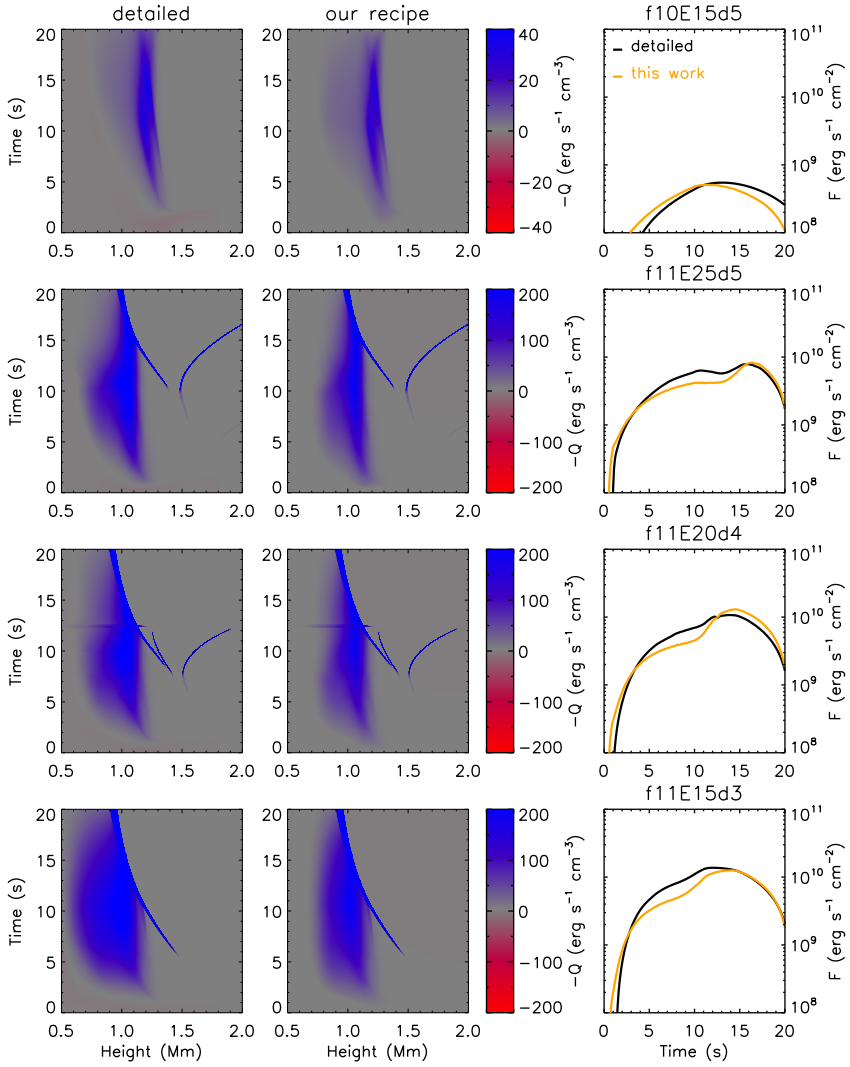

Fig. 5. Same as Fig. 4, but for chromospheric radiative losses contributed by H I Balmer to Pfundt continua.

is within our dataset for fitting. The peak electron flux of the other three models is one order of magnitude larger (f11, 10^{11} erg cm^{-2} s^{-1}), with varying values of E_c and δ (Table 1). In Fig. 4 we calculate the detailed radiative losses in four flare models and compare them with the approximate results from different recipes. We also integrate the total radiative losses spatially (from 0.5 Mm to 2.0 Mm) and show their time evolutions. A striking feature of Fig. 4 is that in spite of radiative cooling, there exists strong radiative heating in the atmosphere, which is discussed further in Sect. 3.3.

Generally speaking, the recipe of GF90 underestimates the radiative cooling in the mid-chromosphere (1.0−1.5 Mm), while the radiative cooling is overestimated in the upper chromosphere. The time evolution of the spatially integrated radiative cooling shows multiple peaks, owing to an inaccurate estimation of the radiative cooling near the transition region. As for the recipe of CL12, the radiative cooling is overestimated by up to 1−2 orders of magnitude due to an overestimation of the H I population fraction in the chromosphere. The results from our recipe appear more reasonable, although the estimated cooling can be larger than the actual cooling by a factor of 3−5 in the f11 models (peak electron flux of 10^{11} erg cm^{-2} s^{-1}).

The temporally and spatially integrated total radiative losses from different recipes, as well as corresponding errors in each flare model, are also listed in Table 1. For most flare models, the results from our recipe are the closest to the detailed solutions. The recipe of GF90 can produce an overall good approximation of the integrated total radiative losses, but the height distribution of the radiative losses is quite different from the actual one (Fig. 4). In flare models with a large cut-off energy (E_c = 25 keV) and a large spectral index ($\delta \geq 5$), the radiative cooling is underestimated from our recipe, but remains within the same order of magnitude as the exact value. This is because in these models, specific regions appear trapped between the transition region and the heated chromosphere that have low temperature, high density, and a large ionization degree, and are referred to as "chromospheric bubbles" (Reid et al. 2020). According to our recipe, a low temperature would mean a low ionization degree. Therefore, the column density of H I, Ca II, and Mg II would be overestimated and the radiative losses are underestimated.

3.3. Radiative heating

As can be seen in Fig. 4, there are regions where the radiative flux contributes to the internal energy as radiative heating through absorption of photons emitted from nearby regions. These regions are always adjacent to the regions with large radiative cooling (Machado et al. 1980; Carlsson & Leenaarts 2012). The magnitude of radiative heating in specific regions is

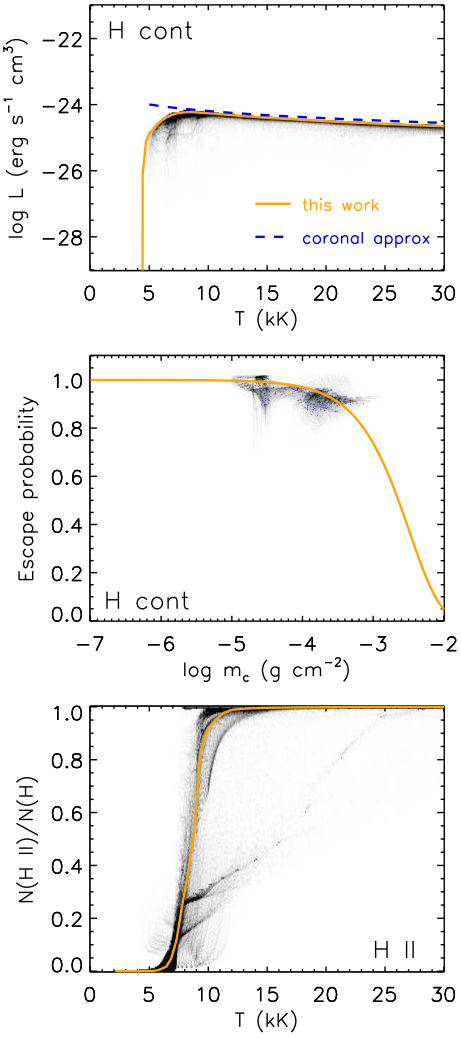

Fig. 6. Probability density functions of the thin radiative loss function and the escape probability for H continua (Balmer to Pfundt), as well as the population fractions of H II, as functions of temperature and column mass. Orange lines show the adopted fit, and the blue dashed curve in the *top panel* shows the thin radiative loss function under coronal approximation.

proportional to the magnitude of radiative cooling in the regions adjacent to them. In flares, radiative heating is mainly contributed by Lyα and the Lyman continuum, as well as the resonance lines of Ca II and Mg II. The contribution of Lyα dominates at the beginning of flare heating, while at a later time, the contribution of the Lyman continuum dominates. Heating from the Ca II H/K lines is partly compensated by cooling from the Ca II triplet lines.

Our recipe, as in the previous ones, does not consider the contribution of radiative heating. It is a great challenge to include both radiative cooling and radiative heating together in one unified empirical formula, because it is very difficult to locate the region of radiative heating. There seems to be no quick method to determine whether the atmosphere at each height is radiatively heated or cooled. However, we do find that for flare models with the same energy cutoff E_c, the location of the radiative heating region is roughly the same. Therefore, for a specific E_c, one might get an empirical relation by fitting both positive and negative escape probabilities together, but this relation is not valid for other values of E_c, and it is not applicable to actual self-consistent magnetohydrodynamic simulations.

Table 2. Total radiative fluxes of the chromosphere from H continua (Balmer to Pfundt) in different flare models.

Flare model	$\mathcal{F}^{\rm tot}_{\rm cont}$ (10^9 erg cm^{-2}) detailed	this work	$\Delta\mathcal{F}^{\rm tot}_{\rm cont}$ (%) this work
Models for fitting			
f10E05d3	9.00	8.36	−7.09
f10E10d3	11.05	8.55	−22.62
f10E15d3	14.59	10.82	−25.88
f10E20d3	17.81	12.91	−27.55
f10E25d3	21.48	15.37	−28.44
f10E05d4	5.40	6.33	17.27
f10E10d4	7.42	7.03	−5.22
f10E15d4	8.97	7.76	−13.45
f10E20d4	12.24	10.08	−17.66
f10E25d4	16.17	12.92	−20.07
f10E05d5	3.76	4.81	27.80
f10E10d5	6.04	6.44	6.48
f10E15d5	6.08	5.84	−3.88
f10E20d5	8.98	7.93	−11.70
f10E25d5	12.56	10.62	−15.57
f10E05d6	2.93	3.93	34.19
f10E10d6	5.40	6.09	12.83
f10E15d6	4.53	4.60	1.62
f10E20d6	7.10	6.62	−6.87
f10E25d6	10.44	9.11	−12.82
f10E05d7	2.48	3.45	39.01
f10E10d7	5.01	5.83	16.38
f10E15d7	3.78	3.85	2.11
f10E20d7	5.98	5.77	−3.48
f10E25d7	9.10	8.11	−10.84
Models for test			
f11E15d3	147.04	122.94	−16.39
f11E20d4	109.77	110.19	0.38
f11E25d5	87.93	76.61	−12.87

Incident radiation of the optically thin radiative losses from the corona can also heat the chromosphere (Wahlstrom & Carlsson 1994; Allred et al. 2015). In flares, the magnitude of incident radiation energy could be comparable to the amount of radiative losses from spectral lines (Hawley & Fisher 1994; Allred et al. 2005). An approximation method for this heating is described in CL12.

3.4. Cooling from Balmer and higher continua

Both the above recipe and CL12 do not include cooling from Balmer and higher continua, because they are optically much thinner than the H I lines and Lyman continuum and the treatment of a unified escape probability curve is not reasonable. Their contributions to the radiative losses are shown in Fig. 5. For flare cases, the region with large cooling from Balmer and higher continua lies below the region with large cooling from H I lines and Lyman continuum, as shown in previous calculations (Avrett et al. 1986; Hawley & Fisher 1994; Procházka et al. 2019). In these cases, radiative heating from Lyα and Lyman continuum is compensated by radiative cooling from Balmer and higher continua to some extent.

We list the values of spatially and temporally integrated radiative losses from Balmer and higher continua for different flare models in Table 2. We find that the total cooling from

Balmer and higher continua can be larger than the total cooling from H I lines and Lyman continuum, especially when the chromosphere is heated after a certain time (Avrett et al. 1986; Hawley & Fisher 1994; Procházka et al. 2019). Although the recipe of GF90 is constructed over the semi-empirical models, it seems that cooling from H I continua is not estimated accurately. Therefore, it would be very beneficial to correctly include cooling from Balmer and higher continua.

Radiative cooling from these continua can be approximated with Eq. (3) in a similar way. The PDFs of the thin radiative loss function and the escape probability are shown in Fig. 6 with fitted curves. The ionization fraction of H II is also fitted accordingly. The escape probability for continuum photons is close to 1 in the chromosphere, while deep down in the photosphere the probability decreases to $e^{-\tau}$, where τ is an approximated optical depth at these continua. We set τ proportional to column mass m_c: $\tau = \alpha m_c$, and a least-square best fit to the PDF gives $\alpha = 3.05 \times 10^2$. The calculated radiative cooling from Balmer and higher continua is also shown in Fig. 5 and Table 2, and it turns out to be a good approximation.

3.5. Cooling from other sources

In our recipe, we only consider H, Ca, and Mg as cooling sources in the chromospheric energy balance. Anderson & Athay (1989) showed that in the quiet Sun, the abundant iron lines can also contribute significantly to the total radiative losses. Their contributions in flare conditions might also be important, because the near-ultraviolet Fe II lines are also enhanced during flares (Kowalski et al. 2017; Graham et al. 2020). Other candidates include the strong He I 10 830 Å line in flares, which is formed in the mid to upper chromosphere and modulated by the incident coronal radiation (Ding et al. 2005; Golding et al. 2014; Kerr et al. 2021). Further investigation is required to quantify the contributions from these lines.

4. Conclusion

In this paper, we provide a new recipe to calculate the chromospheric radiative losses based on the recipe of CL12 but for a flaring atmosphere. We redo the fittings from a grid of flare models and tabulate the three parameters: optically thin radiative loss, escape probability, and ionization fraction as functions of temperature or column density. The largest difference between our recipe and CL12 lies in the empirical curve of ionization fraction. In the 10^4 K temperature plateau of the flaring chromosphere, hydrogen is mostly ionized as a result of increased collisional ionization rates.

The calculated radiative cooling from our recipe is a good approximation of the actual cooling in flares, especially in regions with large cooling values, while GF90 and CL12 tend to under- and overestimate the cooling rate, respectively. It is noted that the H I Balmer and higher continua could also contribute significantly to the radiative cooling in flares, and they can be approximated in a similar way. Our recipe is valid for flares with nonthermal electron peak fluxes in the range of 10^{10}–10^{11} erg cm^{-2} s^{-1}. Nevertheless, our recipe is not designed for all kinds of solar activities, and so it might not work well under atmospheric conditions that are far from flare conditions.

Currently, in our recipe we are unable to consider radiative heating from Lyα and the Lyman continuum, and further study is required to determine how much influence there would be if radiative heating in the flaring chromosphere were neglected.

Acknowledgements. This work was supported by National Key R&D Program of China under grant 2021YFA1600504 and by NSFC under grants 11903020, 11733003, and 12127901, and by the Research Council of Norway through its Centres of Excellence scheme, project number 262622, and through grants of computing time from the Programme for Supercomputing.

References

Allred, J. C., Hawley, S. L., Abbett, W. P., & Carlsson, M. 2005, ApJ, 630, 573
Allred, J. C., Kowalski, A. F., & Carlsson, M. 2015, ApJ, 809, 104
Anderson, L. S., & Athay, R. G. 1989, ApJ, 346, 1010
Avrett, E. H., Machado, M. E., & Kurucz, R. L. 1986, in The Lower Atmosphere of Solar Flares, eds. D. F. Neidig, & M. E. Machado, 216
Bradshaw, S. J., & Cargill, P. J. 2013, ApJ, 770, 12
Carlsson, M., & Leenaarts, J. 2012, A&A, 539, A39
Carlsson, M., & Stein, R. F. 1992, ApJ, 397, L59
Carlsson, M., & Stein, R. F. 1995, ApJ, 440, L29
Carlsson, M., & Stein, R. F. 1997, ApJ, 481, 500
Carlsson, M., & Stein, R. F. 2002, ApJ, 572, 626
Del Zanna, G., Dere, K. P., Young, P. R., & Landi, E. 2021, ApJ, 909, 38
Dere, K. P., Landi, E., Mason, H. E., Monsignori Fossi, B. C., & Young, P. R. 1997, A&AS, 125, 149
Ding, M. D., Li, H., & Fang, C. 2005, A&A, 432, 699
Fang, C., Henoux, J. C., & Gan, W. Q. 1993, A&A, 274, 917
Gan, W. Q., & Fang, C. 1990, ApJ, 358, 328
Golding, T. P., Carlsson, M., & Leenaarts, J. 2014, ApJ, 784, 30
Graham, D. R., Cauzzi, G., Zangrilli, L., et al. 2020, ApJ, 895, 6
Gudiksen, B. V., Carlsson, M., Hansteen, V. H., et al. 2011, A&A, 531, A154
Hawley, S. L., & Fisher, G. H. 1994, ApJ, 426, 387
Kerr, G. S., Allred, J. C., & Polito, V. 2020, ApJ, 900, 18
Kerr, G. S., Xu, Y., Allred, J. C., et al. 2021, ApJ, 912, 153
Kowalski, A. F., Allred, J. C., Daw, A., Cauzzi, G., & Carlsson, M. 2017, ApJ, 836, 12
Leenaarts, J., Carlsson, M., & Rouppe van der Voort, L. 2012, ApJ, 749, 136
Leenaarts, J., Pereira, T. M. D., Carlsson, M., Uitenbroek, H., & De Pontieu, B. 2013, ApJ, 772, 89
Machado, M. E., Avrett, E. H., Vernazza, J. E., & Noyes, R. W. 1980, ApJ, 242, 336
Nagai, F. 1980, Sol. Phys., 68, 351
Pereira, T. M. D., & Uitenbroek, H. 2015, A&A, 574, A3
Polito, V., Testa, P., Allred, J., et al. 2018, ApJ, 856, 178
Procházka, O., Reid, A., & Mathioudakis, M. 2019, ApJ, 882, 97
Reid, A., Zhigulin, B., Carlsson, M., & Mathioudakis, M. 2020, ApJ, 894, L21
Uitenbroek, H. 2001, ApJ, 557, 389
Wahlstrom, C., & Carlsson, M. 1994, ApJ, 433, 417
Wang, Y., & Yokoyama, T. 2020, ApJ, 891, 110